A Novel Automatic Monitoring and Control System For Induced Jet Breakup Fabrication of Ceramic Pebbles

Miao Zhang[1][a], Oliver Leys[2][b], Markus Vogelbacher[1][c], Regina Knitter[2][d] and Jörg Matthes[1][e]
[1]*Institute for Automation and Applied Informatics, Karlsruhe Institute of Technology, Hermann-von-Helmholtz-Platz 1, Eggenstein-Leopoldshafen, Germany*
[2]*Institute for Applied Materials, Karlsruhe Institute of Technology, Hermann-von-Helmholtz-Platz 1, Eggenstein-Leopoldshafen, Germany*

Keywords: Ceramic Pebbles Manufacturing, Control System, High-Speed Camera Based Measurement System, Melt-Based Process, Real-Time Measurement and Control.

Abstract: As the production of lithium-rich ceramic pebbles play a key role in the tritium-breeding blankets, it is vital for future fusion reactors. To ensure high-quality pebbles, the Karlsruhe Institute of Technology (KIT) has developed a melt-based fabrication process called KALOS (KArlsruhe Lithium OrthoSilicate). This process involves the break-up of a molten laminar jet to produce pebbles with precise diameters of hundreds of micrometers, which are highly dependent on process parameters. Therefore, a real-time monitoring and regulation system is essential for the fabrication process. This paper discusses a high-speed camera-based measurement system designed to automatically monitor and control the production process. Experimental evidence shows that this system can accurately provide real-time data on the sizes, locations, and distance distribution of the molten ceramic droplets utilizing image processing approaches. Additionally, the system is capable of controlling the production of pebbles by adjusting the driving frequency in real-time based on real-time measurements of the computer vision.

1 INTRODUCTION

Over the past few decades, nuclear fusion has gained significant interest as a sustainable energy source for future generations, primarily due to its safety and the minimal amount of long-term radioactive waste it produces. A key step in nuclear fusion is the production of its two fuel components: deuterium, which can be extracted from seawater, and tritium, which must be generated on-site to ensure the reactor's self-sufficiency and allow steady-state operation. To produce the necessary tritium, it is proposed to install lithium-rich ceramic pebbles in the reactor walls, forming pebble beds within solid breeder blankets (Knitter et al., 2013)(Hernández et al., 2018). During the fusion of tritium and deuterium, highly energetic neutrons collide with these ceramic pebbles, causing the lithium to transmute into helium and tritium. The tritium is then processed and recirculated to react with deuterium.

To address the demand for tritium breeding ceramics, various processing techniques have been developed globally. For instance, Lulewicz and Roux utilized an extrusion-spherodisation technique to produce pebbles. Park *et al.* (Park et al., 2014) successfully fabricated Li_2TiO_3 pebbles using a slurry droplet wetting method. Cai *et al.* (Cai et al., 2022) introduced a piezoelectric micro-droplet jetting approach to create Li_2TiO_3 green pebbles, which are subsequently sintered. Additionally, Hoshino developed a pebble production process based on an emulsion method, and 3D printing has also been proposed for fabricating tritium breeding structures.

At the Karlsruhe Institute of Technology (KIT), the KALOS process was developed to produce advanced ceramic breeder pebbles by breaking up a molten laminar jet and solidifying it with liquid nitrogen (Heuser et al., 2018)(Leys et al., 2021). These pebbles, made of lithium orthosilicate with a strengthening phase of lithium metatitanate, are considered the solid EU-reference material for tritium breeding.

[a] https://orcid.org/0000-0002-3642-2024
[b] https://orcid.org/0000-0001-8814-3011
[c] https://orcid.org/0000-0002-8622-8254
[d] https://orcid.org/0000-0002-3126-1356
[e] https://orcid.org/0000-0002-0963-6000

Zhang, M., Leys, O., Vogelbacher, M., Knitter, R. and Matthes, J.
A Novel Automatic Monitoring and Control System For Induced Jet Breakup Fabrication of Ceramic Pebbles.
DOI: 10.5220/0013665600003982

In *Proceedings of the 22nd International Conference on Informatics in Control, Automation and Robotics (ICINCO 2025) - Volume 1*, pages 25-36
ISBN: 978-989-758-770-2; ISSN: 2184-2809

The melt-based process offers several advantages, including scalability to meet future reactor demands and the ability to recycle pebbles without wet-chemical processing (Leys et al., 2016). Compared to the previous melt-spraying process (Knitter et al., 2007), the laminar jet break-up provides better control over droplet size and, consequently, the pebble size distribution.

The efficiency of breeder blankets, and consequently the fuel cycle, relies on achieving a high pebble packing factor to maximize bulk lithium density. At KIT, pebbles are produced within a size range of 250 to 1250 µm, which is expected to ensure a high packing factor in the complex geometries of breeder blankets. The KALOS process involves the break-up of a molten laminar jet due to Plateau-Rayleigh instabilities, where surface tension forces eventually overcome viscous forces, causing a droplet to break off. Typically, these instabilities are caused by random ambient disturbances. However, by using specific driving frequencies, the process can be directly influenced, thereby controlling the jet break up and consequently the size distribution of the pebbles. This refinement has led to higher process yields and increased monodispersity of the pebbles.

As a purpose to study and quantify the jet break-up characteristics, a high-speed camera system with an image-processing algorithm was developed. An index called the coefficient of variation (CV) was introduced to measure the regularity of the jet break-up, with a lower CV indicating a more regular and stable break-up and higher monodispersity. By adjusting the disturbance frequency on the jet, a low CV value can be achieved, ensuring stable and regular jet break-up and the production of pebbles within the desired size range. This study explores the beneficial frequency range for jet break-up and implements a feedback mechanism in the process control to maintain a low CV value.

Therefore, this paper introduces a novel automatic high-speed camera-based system that can monitor and control the production of ceramic pebbles in real-time. The paper is organized as follows: Section 2 presents the theoretical foundation of jet break-up and the fabrication procedure of ceramic pebbles. The high-speed camera-based measurement system, including the image processing algorithms, is illustrated in Section 3. Section 4 focus on the automatic control system of the droplet generation frequency to ensure stable pebble fabrication. Section 5 presents and discusses the results of the introduced automatic monitoring and control system. Section 6 concludes the paper.

2 FABRICATION OF CERAMIC PEBBLES

As mentioned in the first section, the ceramic pebbles are produced using the KALOS process, which relies on the break-up of a molten laminar jet. This section details the advanced pebble fabrication process including the corresponding theoretical basis for jet break-up.

The KALOS process produces ceramic pebbles based on the break-up of the molten jet that is caused by the growth of Plateau-Rayleigh instabilities. These disturbances manifest as sinusoidal waves on the jet's surface. When the wave amplitude reaches a certain threshold, surface tension forces surpass viscous forces, resulting in a droplet detaching from the jet. In the KALOS process, disturbances are introduced to the jet by vibrating the process pressure at selected driving frequencies to control jet break-up and droplet generation. Since the jet velocity (v) and radius (r) remain constant during production, the applied frequency is directly related to the wavenumber. Only frequencies within a specific range will influence the jet break-up, with an optimal frequency corresponding to the wavenumber that promotes the fastest growth of disturbances. Within this range, the applied disturbances suppress ambient noise, leading to a more controlled and uniform jet break-up. At the optimal frequency, disturbance waves grow the fastest, resulting in the most uniform break-up and the smallest coefficient of variation (CV) value. The CV value is defined as the normalized standard deviation of the droplet spacing:

$$CV = \frac{\sigma(s)}{\mu(s)} \tag{1}$$

where s is the droplet spacing, $\sigma(s)$ its variance and $\mu(s)$ its mean value. The CV value is one of the most vital indexes for indicating the production quality. A smaller CV value represents a more stable fabrication process and a higher production quality. Another measure of production quality is the size of the droplets.

In the KALOS process, starting powders are pre-reacted to form a composition of 70 mol% Li_4SiO_4 and 30 mol% Li_2TiO_3, which is then placed into a platinum alloy crucible. As shown in Figure 1, the crucible is heated in a furnace to approximately 1400 °C for creating a melt. Meanwhile, a pressure of 320 mbar is applied to the crucible, forcing the melt through a small nozzle (300 µm diameter) at the bottom, forming a laminar jet. This jet breaks up into droplets, which exit the furnace and enter a cooling tower, where they are solidified using liquid nitrogen.

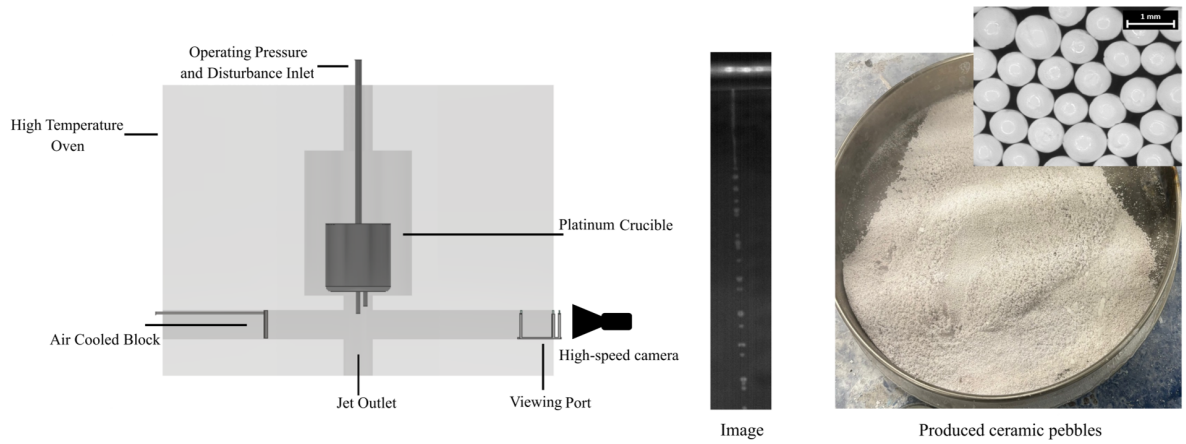

Figure 1: High-temperature KALOS production experimental set-up and the gathered pebbles (Zhang et al., 2024).

The pebbles are then collected at the base of the tower and transferred to the laboratory for characterization. An example of the produced pebbles is shown in Figure 1 on the right.

In addition, Figure 1 also includes an image captured by the high-speed camera in the middle, demonstrating the camera system's ability to clearly capture the droplets, which is crucial for the measurement system. The gathered pebbles after cooling (i.e., the solidified droplets) are then analyzed in terms of their sizes and size distributions using a particle analyzer "HAVER CPA 2-1" by Haver & Boecker, Germany. The analysis allows for a quantitative validation of the presented high-speed camera based measurement system.

3 COMPUTER VISION BASED MEASUREMENT SYSTEM FOR MONITORING THE PEBBLES FABRICATION

As introduced in the previous section, the quality of the jet break-up based ceramic pebbles fabrication is indicated by two measures: the size of the generated droplets and their coefficient of variation (CV) values. To ensure the production quality, a measurement system to evaluate the droplet formation in real-time, focusing on these two measures, has been developed. The measurement system includes hardware setup and image processing approaches that are featured in the following.

3.1 High-Speed Camera System

The major component of the measurement hardware is a high-speed camera (Optronis CP70-1-M-1000), which is able to achieve a frame rate of approximately 1000 frames per second (fps) at a maximum resolution of 1280×1024 pixels. By selecting a region of interest and excluding unnecessary image areas, the image size can be reduced, significantly increasing the maximum possible frame rate. The camera and the applied telecentric lens are mounted on the side of the high temperature test facility and monitor the droplet formation via a port of special glasses combination, as schematically illustrated in Figure 2. The camera is arranged in the upper part of the furnace so that it can observe the droplet formation directly at the crucible nozzle.

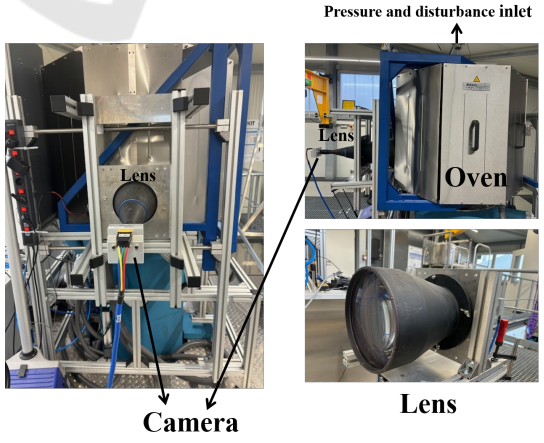

Figure 2: High temperature test facility and the applied high-speed camera system.

A cooled plate is mounted behind the jet to sim-

plify identification of the jet and droplets, as it can provide sufficient light contrast. For the KALOS process, the optical sensor's active area measures 8.448 mm × 6.758 mm, with a pixel size of 6.6 µm × 6.6 µm. Calibration indicates that one pixel in image coordinates corresponds to an actual size of approximately 71.94 µm × 71.94 µm. The high-speed camera allows for an exposure time as short as 2 µs, enabling clear recording of rapid jet break-up processes and reducing motion blur. To balance for illuminating the produced droplets while maintaining their spherical shape, the exposure time was set to 160 µs. The utilized telecentric lens is a specialized optical component designed to maintain a consistent magnification across varying object distances. Due to its low aberration and stable magnification properties, it is particularly well-suited for applications requiring high-precision dimensional measurements, such as monitoring micron-sized droplets. Detailed technical parameters of the camera and lens are provided in Table 1.

Table 1: Technical details of the high-speed camera and lens.

Camera	Optronis CP70-1-M-1000
Max. resolution	1280x1024 px
Frame rate for max. resolution	1040 fps
Frame rate for 1/4 max. resolution	3800 fps
Pixel size	6.6 µm
Exposure time	2 µs-1/frame rate
Lens	TC23172
Working distance	526.9 mm
Depth of filed	159.2 mm

For the measurement, the camera system captures the scene in the form of an image sequence with temporally continuous images. The measurement system analyses the image sequence to compensate the random fluctuation of individual image. The analysing of one image sequence corresponds to a measuring cycle.

3.2 Image Processing

After capturing the image sequences, each individual image of a sequence is processed with image processing approaches to compute the production quality parameters. The presented measurement system mainly includes the determining of the nozzle position, the detection of the jet, and the identification of generated droplets, as schematically depicted in Figure 3. Under the consideration that the nozzle position is basically unchanged, the nozzle detection is performed only once for one image sequence to enhance the computation efficiency. Meanwhile, the detection of the jet and droplets occurs in all images within the sequence to ensure an accurate measurement of the production parameters.

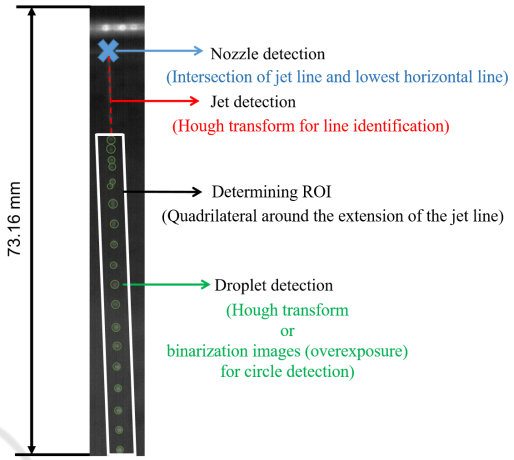

Figure 3: Image processing tasks of the high-speed camera based measurement system.

Obviously, the most crucial task of this measurement system is to detect the size, amount and position of the droplets. To accurately localize the droplets and minimize background noise, the nozzle and jet are detected at first, which helps to constrain the region of interest (ROI) for droplet detection. Only droplets near the jet extension are identified, reducing non-droplet detections from the background and speeding up the processing to ensure real-time detection. In our study, the jet is treated as a line with an angle of up to $\pm 10^{\circ}$ from the vertical direction. Around the jet line, ROI is defined as a quadrilateral, whose top and bottom sides are horizontal, while the left and right sides are parallel to the jet line. The top line of the ROI is at the end of the jet detection, while the bottom line corresponds to the end of the entire image. The left and right sides are staggered by a certain pixel distance to the detected jet on the left and right, as presented in Figure 3. The jet line is detected using the Hough transform (Hart, 2009). Principally, the nozzle's location is considered the starting point of the jet. For accuracy, the nozzle is identified as the intersection of the jet line with the lowest horizontal line that is also identified by the Hough transform. Afterward, the ROI can be determined and the droplets inside the ROI are detected by various methods in accordance with the experient conditions.

Within the detected ROI, the droplets can be identified with the help of a Hough transformation or im-

age binarization. The Hough transform is a feature extraction technique that identifies objects through a voting process taking place in a parameter space (Hart, 2009). Initially designed for detecting line segments in images, the Hough transform is well-suited for jet detection. Over time, the classical Hough transform has been extended to recognize various shapes, such as circles (Ballard, 1981). For the introduced measurement, two form detection methods are integrated: the Hough transform and image binarization. In the context of droplet detection, the Hough transform demonstrates superior performance in terms of robustness and accuracy due to its relative insensitivity to individual pixel grey values. Nevertheless, the precision of localizing detected shapes using the Hough transform is highly dependent on the regularity of these shapes. When shapes deform for reasons such as exposure time, the Hough transform's localization can become biased, significantly affecting the determination of the CV value. To address this issue, the measurement system also contains an alternative function for detecting droplets based on binary images in special cases. For droplet detection using binary images, each image of a sequence is binarized by the Otsu threshold selection method, which performs automatic image thresholding based on the grey value distribution of the image (Otsu, 1979). Subsequently, the circle forms are identified according to the connectivity of the foreground after binarization (Haralick and Shapiro, 1992). As mentioned, the binarization detection approach is designed to make up for the deficiency of the Hough transform in dealing with irregular shapes as a consequence of overexposure. Therefore, the choice of detection method in practical application (KALOS process) depends on the exposure time. The system switches to this alternative method when the required exposure time exceeds 500 µs.

For the measurement system, the droplet diameter can be directly introduced by the circle detection approaches, while the CV value needs computing following in line with the definition of equation 1. The standard deviation of the droplet spacing ($\sigma(s)$) is denoted as:

$$\sigma(s) = \sqrt{\frac{1}{N-1}\sum_{i=1}^{N}(s_i - \mu(s))^2}, \tag{2}$$

and the average spacing $\mu(s)$ is computed as:

$$\mu(s) = \frac{1}{N}\sum_{i=1}^{N} s_i \tag{3}$$

Before computing the CV value, the detected droplets are rearranged from top to bottom according to their positions, then the distance between neighbouring droplets are calculated and noted as s_i. Hereby, i represents the ith droplet spacing of the N spacing for $N+1$ droplet detections. To compensate for the fluctuations of the results based on individual images, the measurement system outputs the average CV value of an image sequence with M images as:

$$\sigma = \frac{\sum_{j=1}^{M}\sigma(j)}{M}. \tag{4}$$

4 AUTOMATIC CONTROL SYSTEM

As introduced in the previous sections, the CV value indicates the regularity of the molten jet break-up and is thus the most crucial parameter in ceramic pebble production. The present control system applies the CV value as the control foundation. Albeit theoretically, frequencies within a certain range should enhance the jet break-up regularity (thereby lowering the CV value), empirical studies have demonstrated that the CV value's response to driving frequency can be irregular (Leys et al., 2019). Even within the effective frequency range, instances indicate that the CV value abruptly increases at several frequencies. It is hypothesized that these frequencies correspond to resonances within the system, which subsequently cause a more irregular jet break-up. To ensure the regularity of the droplets generation and the quality of the pebbles fabrication, a real-time control system for adjusting the driving frequency is necessary. Once the CV value surpasses a predetermined threshold, the control system is able to adapt the frequency to facilitate the stability of the droplet generation. With the integration of the control system, the ceramic pebbles fabrication can be automatically monitored and controlled in real-time. The complete schematic representation of this process is shown in Figure 4.

As illustrated in Figure 4, the measured CV value is transferred from the measurement system to the control system, which then regulates the driving frequency. Afterward, the to be adjusted frequency value is passed to LabVIEW, which can implement the adjustment of the process parameter according to the control system. In addition, LabVIEW also displays the process parameter and the measurement results in real time. Therefore, LabVIEW is interpreted as a visualization and operating system for the entire production. The measurement system, the control system, and the operating system work together to realize the closed-loop monitoring and control of the entire production process. This section concentrates on

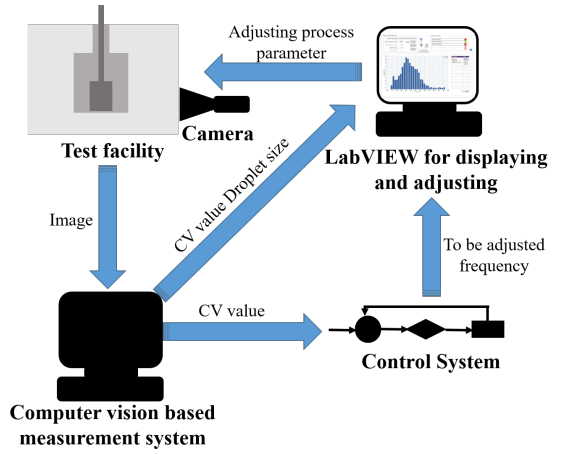

Figure 4: Schematic of the introduced measurement systems and control systems for monitoring and controlling the KALOS process.

the control system.

Figure 5 provides an overview of the control logic. A small value of CV indicates a sufficient quality of the droplet generation. When the measured CV value exceeds a predefined threshold, the current driving frequency requires adjustment. In line with the theory, the optimal frequency for a specific production should not vary significantly from the principal optimum. Typically, each process setup has several fixed optimal driving frequencies, and adjustments are usually minor. Thus, a range of variation is defined in the control system as well. If the frequency adjustments fail to reduce the CV value to the desired threshold within acceptable limits, the system will alert the operator to inspect the nozzle for potential issues. Under these circumstances, the problem is most likely caused by the nozzle (for instance, the nozzle being affected by the melt), not the driving frequency of the process.

Initially, the system selects an initial frequency determined by theory and empirical observation. In the KALOS process this initial frequency is set as 1000 Hz. The measuring system measures then the corresponding CV value at 1000Hz. Thereafter, the system chooses a frequency between 750 and 1000 Hz and measures the corresponding CV value. Subsequently, a frequency between 1000 Hz and 1250 Hz is chosen and the corresponding CV value is measured. Based on these three known frequencies and corresponding measured CV values, a quadratic polynomial is fitted to more accurately determine the optimal frequency value. The minimum point of the computed quadratic polynomial (i.e., the smallest approximated CV value) is calculated and its corresponding frequency is utilized as a new driving frequency. After measuring the CV value for this frequency, the polynomial fit is repeated based on four points and the driving frequency is again adapted to the frequency of the new minimal CV value. This iterative procedure stops when the frequency change significantly slows down, because under this condition, adding more CV values at additonal frequencies to the polynomial fitting provides only a slight benefit. The system then switches to a more sophisticated algorithm to find the optimum. With the help of polynomial fitting, the control system can limit the regulation range within a certain area, which benefits the regulation efficiency and reduces the control time. The system regards the minimizer of the quadratic polynomial as the initial value to determine the final optimal frequency by applying the global optimum finding solution. The applied global search algorithm is the simulated annealing (van Laarhoven and Aarts, 1987). Compared to other global optimum searching methods, such as the Burg Algorithm (Orfanidis, 1985) and the Particle Swarm Optimization (Pedersen, 2010), the simulated annealing algorithm shows its merits in the global search capability, the high adaptability, and its simple implementation. The Burg Algorithm is primarily used for spectral estimation and signal processing, which is suitable for handling time series data and not appropriate for combinatorial optimization problems (Vos, 2013).The Particle Swarm Optimization optimizes problems by simulating group behavior, which is adequate for continuous optimization problems (Bonyadi and Michalewicz, 2017). Since PSO shows accurate performance in searching large spaces, it can get trapped in local optima.

The technique of simulated annealing is based on the parallelism between the problem of finding the minimum of a function and the phenomenon of annealing in statistical mechanics (Banchs, 1997). After measuring the CV value corresponding to the initial frequency, which is determined by the polynomial fitting, the simulated annealing then randomly generates a new solution in the neighborhood of the current solution. Subsequently, the CV value of the new solution is compared with the last CV value. If the new CV value is smaller than the previous one, the new frequency is accepted. Otherwise, a probability determined by the Metropolis criterion (Metropolis et al., 1953) is computed, as:

$$P = \exp\left(-\frac{\Delta CV}{f}\right), \tag{5}$$

where ΔCV is denoted as the CV value difference and f is the utilized frequency. The new solution with a higher CV value is accepted with this probability. Afterward, the driving frequency is adjusted again by a step of

$$f_{new} = \alpha \cdot f. \tag{6}$$

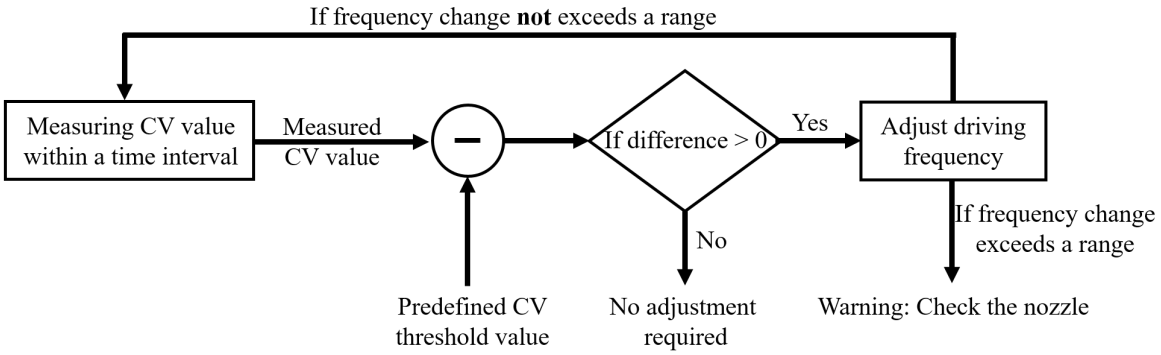

Figure 5: Schematic of the control logic.

For the present control system, α is defined as a random value from a normal distribution with the average value of 0 and a standard deviation of 0.01. The iteration stops when the frequency reaches a certain threshold or the maximum number of iterations is reached. The control system then ouputs the frequency with the lowest found CV value. By implementing these steps, the simulated annealing (SA) algorithm can effectively escape local optima (Delahaye et al., 2018). Nevertheless, for a real-time control system, where an optimum is desired in a possible short time, the SA algorithm alone without restricting the search area in advance is inappropriate, since it requires costly computational time to ensure its functionality. Thus, we combine a polynomial fitting together with SA algorithm to realize a sufficient accuracy in an acceptable time.

If the control system is not activated to function at the very beginning, but is triggered by a CV value exceeding the threshold during production, the polynomial fitting is initialized to the current frequency, followed by a new frequency randomized within 250 Hz to the left and right of it.

In addition, in order to ensure that the KALOS process has sufficient response time to frequency changes, the measurement system usually captures several image sequences before conducting the measurement, which is controlled by the measurement signal.

5 RESULTS AND DISCUSSION

The image processing techniques and control system are outlined in the previous sections. This section presents and discusses the results of these methods. For the computer vision based measurement system, the two crucial parameters, i.e., the CV values and the molten ceramic droplets' diameters, are computed. For the purpose of validating the performance of the high-speed camera based measurement system, the gathered pebbles after cooling are analyzed in terms of their diameters, which can be compared with the measurement outputs to evaluate the accuracy of the system. For the control system, the control process and the intermediate frequencies are visualized to follow the frequency adjustments.

5.1 Computer Vision Based Measurement System

At first, droplets are generated by applying driving frequencies ranging from 0 to 5000 Hz to provide an overview of the frequency's effects. According to extensive experimental data and theoretical foundations, frequencies above 3000 Hz barely affect the jet breakup. Thus, frequency ramps from 0 to 5000 Hz were used to study the frequency effects, ensuring the entire range of influence was covered. Figure 6 displays images of the jet break-up captured by the high-speed camera at a frame rate of 500 fps over three minutes.

With a gradually increasing driving frequency, the average diameter increases and then decreases. The change in the CV value is not easily discernible from the figure. The smallest CV value is observed at a driving frequency of around 1000 Hz. To achieve a more visible observation of the impact of the driving frequency on the CV value and droplet diameter, the results of the image processing are presented in Figure 7. The horizontal axis represents the driving frequency, while the vertical axis shows the CV and diameter, respectively. Each green point corresponds to the CV value or median diameter based on a single image (frame) generated by the corresponding frequency. For statistical observation, the data are smoothed by a robust linear regression (Andersen, 2008) over a window of 200 frames that are presented by the black lines in the figure.

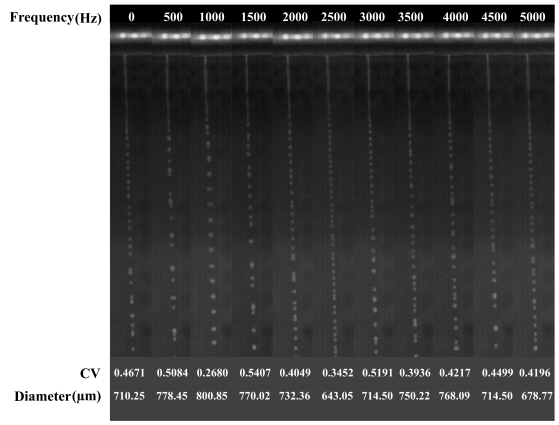

Figure 6: Effect of the driving frequency on the appearance the molten ceramic jet break-up. The corresponding CV values and droplet diameters (in µm), calculated by the image processing algorithms, are shown at the bottom.

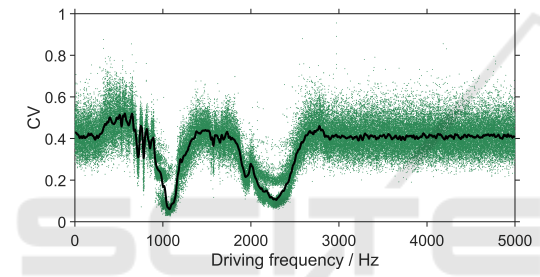

(a)

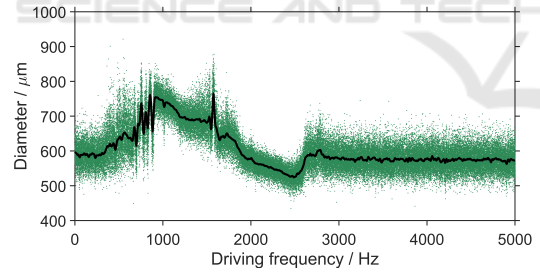

(b)

Figure 7: Output of the measurement system. (a) The CV value and (b) The median diameter of the droplets.

As revealed by Figure 7(a), frequencies between approximately 800 Hz and 2600 Hz affect the jet break-up, and in general, two minima exist: one around 1000 Hz and another at around 2300 Hz. Between these two minima, internal resonances disturb the jet break-up, as indicated by the irregular jet break-up images at 1500 Hz and 2000 Hz in Figure 6. As for the impact of the driving frequency on the droplet diameter, at a driving frequency of 1000 Hz, droplets with diameters of approximately 750 µm are formed, while at 2500 Hz, droplets with diameters of 550 µm are produced. Apparently, the diameter decrease linearly from 1000 Hz to 2500 Hz. Again, resonances in the system are evident around 1500 Hz, where there is a greater variation around the smoothed data value. As proved by Figure 7, the optimum of the CV value occurs at a driving frequency of approximately 1000 Hz, which is also the initial value of the control system. Thereafter, we also conducted experiments to investigate the droplet generation at the driving frequency of 1000 Hz with respect to the droplet diameter.

The measured droplet diameters and the analyzed pebble diameters are presented in Figure 8. In Figure 8 (a), the high-speed camera based measured diameters are depicted in a green histogram in intervals of 5 µm with an approximated normal probability density distribution. The black dashed line stands for the diameter with the highest probability density, while the orange dashed line represents the average diameter of the best fitting normal distribution. As shown in the figure, the diameter with the highest probability occurs in the interval 760 µm to 765 µm, and the average value of the fitted normal distribution is 732.05 µm. The vast majority of the produced droplets are between 500 and 1000 µm in diameter.

To validate the adequacy and accuracy of the proposed measurement system, solidified pebbles after cooling are collected and physically analyzed by a particle analyzer for determining their sizes and distribution, as shown in Figure 8 (b). In the figure, the histogram with larger intervals depicts the distribution of pebble diameters, and the red line marks the cumulative distribution of the pebble diameter. According to the analysis the pebble diameters are primarily focused between 600 µm and 800 µm, and the most probable diameter around 750 µm, matching the measured size of the generated droplets shown in Figure 8 (a). Taking the solidification effects and the physical deformation of the droplets during falling into consideration, which can result in slightly altering of the size between the droplets and the solid pebbles, the pebble size distribution results and the image processing of the jet break-up are in strong agreement, thereby validating the measurement system's accuracy.

5.2 Control System

In order to present the regulation process of the control system more clearly, we select an experiment for validation and show its CV value / frequency curve in Figure 9. In the experiment, the driving frequency varies from 0 to 5000 Hz, and the images are captured with a framerate of 500 fps. Similar to Figure 7 (a), green points represent the CV values for sin-

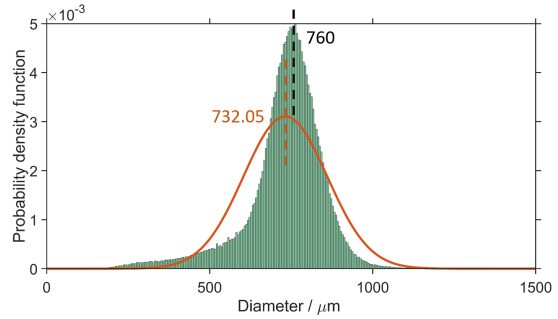

(a)

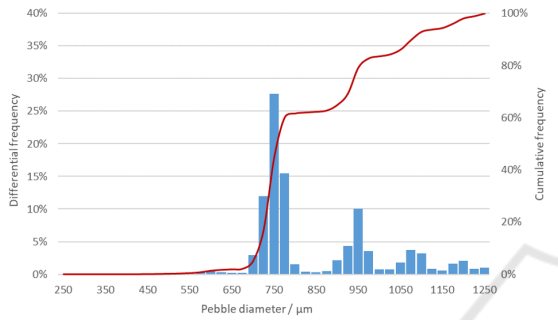

(b)

Figure 8: Diameter of droplets and gathered pebbles at the driving frequency of 1000 Hz. (a) Measured droplet diameters and its distribution. (b) Measured diameter distribution of the pebbles provided by particle analyzer HAVER CPA 2-1.

gle frames generated by the corresponding frequency, while the black line illustrates the smoothed version over a window of 200 frames. Obviously, compared to the experiment displayed in figure 7, this experiment is more difficult to modulate since its CV distribution is more diffuse with a significant fluctuation. Moreover, the CV of this experiment fluctuates drastically at the two local minimum points, i.e., around 1000 Hz and 2000 Hz. Especially around 1000 Hz, the local CV distribution seems disconnected due to the local large variation of CV values, which is primarily caused by suspected internal resonances that lead to irregular jet break-up. In order to explain the situation more visually, two sets of images taken at adjacent frequencies are shown in Figure 10.

Figure 10 shows four images taken at different frequencies. Apparently, the difference occurs when the droplets are first generated. For example, at 1200 Hz, the droplets in the white box are detected as two, whereas at 1201 Hz, in essentially the same image position, the two droplets converge into one large one. A more pronounced difference can be observed at 1260 Hz and 1261 Hz, where the droplet generation is unstable due to the irregularity of jet break-up, which affects the CV value. This phenomenon highlights the

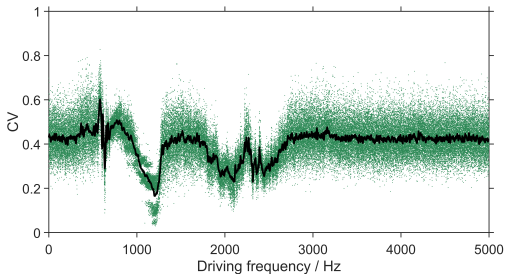

Figure 9: Plot of CV value versus driving frequency for one experiment. Frequency ramp from 0-5000 Hz

need for a control system to manage unknown system responses. In addition, with the help of the waiting time in the control system for waiting the response, some random irregularity can be attenuated to some extent.

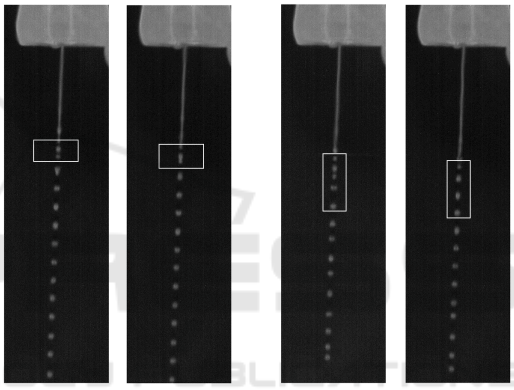

Figure 10: Captured images of adjacent frequencies.

As described in Section 4, we select at first three data points around 1000 Hz and approximate a polynomial approach to these points. Afterward, the input data are updated using the local minimum of each fitted polynomial. The process is detailed in Figure 11. As presented by the figure, the polynomial fitting is repeated five times and stops when the curves only barely vary. The local minimum of the last curve is considered as the inital point for the following global optimization algorithm.

Using the polynomial fitting output as an initial point, the control system performs the simulated annealing algorithm to finalize the optimal frequency. The temporal results of the algorithm during the regulation are shown in Figure 12 and the corresponding detailed values for each adjustment are listed in the Table 2. The control system first adjusts the frequency around the initial value (1114 Hz) and then measures the CV value. Subsequently, according to the algorithm, all frequencies resulting in smaller CV values

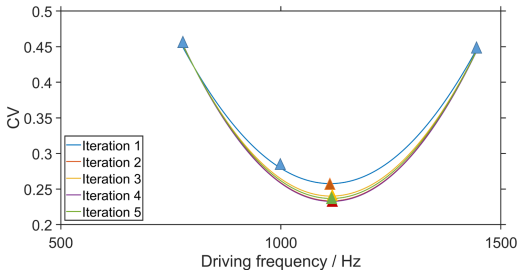

Figure 11: Process of polynomial fitting. Different curves represent different iterations. The triangles in the image are the data points for each fitting, whose colors also identify the number of iteration.

are updated as the new input. Frequencies leading to larger CV values are only accepted with a certain probability to ensure that the local optimum solution is skipped. It should be noted that in Table 2 only the steps that are updated by new frequencies are listed. In several steps, the frequencies are not updated because of increasing CV values.

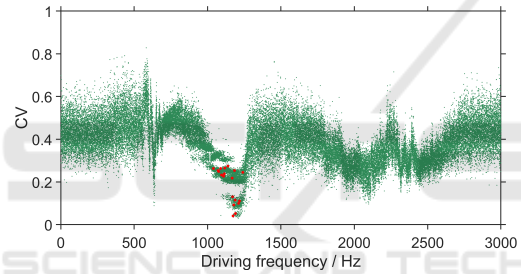

Figure 12: Temporal results of the control output by the simulated annealing algorithm. Green points denote measurement points and red asterisks indicate the data points that are scanned by regulation.

At first, the control system adjusts the frequency at around 1110 Hz, however, the CV value does not decrease significantly. Therefore, the system reduces the frequency to around 1000 Hz. Although the CV value fluctuates, none of them reached the system's threshold, 0.2. Subsequently, the system continues to move the frequency range to around 1200 Hz, where the system detects a very low CV value (already approaching the optimal solution). Thereafter, the system still tries to vary the driving frequency, but none of the resulting CV values reach below this CV value. Additionally, the system starts to converge, i.e., the difference between the measured CV value and the detected minimum value becomes smaller, and then the iteration stops.

Despite the fact that the local minimum has been roughly determined previously by polynomial fitting, the whole control process lasts for several dozen iterations, and since each iteration also requires a corresponding waiting time, the overall duration is the product of the waiting time and the number of iterations. The processing time of each image sequence is about 2 to 3 s, thus, the process lasts about 3 min, which is acceptable in the KALOS process. Obviously, without polynomial fitting, the whole regulation will take much longer, significantly affecting the production.

Table 2: Driving frequency and CV value of each control step.

Iteration	Driving frequency (Hz)	CV
1	1114	0.238
2	1109	0.227
3	1072	0.253
4	1188	0.115
5	1184	0.253
6	1089	0.263
7	1095	0.232
8	1040	0.263
9	1076	0.249
10	1117	0.265
11	1139	0.274
12	1168	0.218
13	1212	0.100
14	1218	0.111
15	1240	0.245
16	1174	0.041
17	1171	0.130
18	1179	0.092
19	1190	0.052

6 CONCLUSIONS

The paper presents a novel high-speed camera based measurement and control system that aims to analyze and control the production of lithium pebbles for fusion reactors automatically. The system, which incorporates image processing techniques, allows for real-time monitoring of the droplet generation process and measuring the droplet diameters and the normalized standard deviation of droplet spacing (CV). The CV value is considered as the most crucial parameter to indicate the fabrication performance, since it directly indicates the regularity of the jet break-up. Moreover, the CV value also guides the adjustment of the driving frequency of the control system. According to the molten jet break-up theory discussed in the second section, a low CV value indicates a regular and stable jet break-up, which is desirable for production. Owing to the introduced measurement system, the study enables the investigation into the influence

of the driving frequency on the CV value and droplet diameter. The experiments are conducted with both varying driving frequency, which provides a broad overview of ceramic droplet production, and a certain frequency. As revealed by the results, the driving frequency significantly affects production performance within a certain range, with the optimal frequency for the utilized nozzle being around 1000 Hz. The experiment under 1000 Hz driving frequency is further examined in detail, and the solid ceramic pebbles under this condition are collected and analyzed by a particle analyzer. By comparing the measured droplet diameters with the analyzed pebble diameters, the accuracy and reliability of the computer vision based measurement system has been proved. Given that generation frequency is a critical parameter for controlling droplet production, the measurement system proves essential for selecting the initial frequency and making further adjustments. If the CV value exceeds a certain value, the driving frequency needs adjustment implemented by the control system to maintain an optimal CV value. For the adjustment, the control system performs a polynomial fitting at first to roughly define an initial minimum, which is regarded as input to the subsequent global optimization algorithm. The utilized algorithm is the simulated annealing, which is widely applied to search global optimum. According to the performance of the algorithm on the experiment, the control system is able to realize real-time control of the system.

Our experiments with the described settings demonstrate the effectiveness of the proposed automatic system in monitoring and controlling ceramic pebble production. Future research will focus on evaluating the system's robustness under different conditions. Additionally, we plan to enhance the image processing techniques to analyze the generation and motion velocity of the produced droplets. By examining the generation speed, we can calculate the quantity of droplets, which will help estimate the efficiency of raw material usage.

ACKNOWLEDGEMENTS

This work has been carried out within the framework of the EUROfusion Consortium, funded by the European Union via the Euratom Research and Training Programme (Grant Agreement No 101052200 — EUROfusion).

REFERENCES

Andersen, R. (2008). Modern methods for robust regression. *Sage University Paper Series on Quantitative Applications in the Social Sciences*, pages 1654–1662.

Ballard, D. (1981). Generalizing the hough transform to detect arbitrary shapes. *Pattern Recognition*, 13(2):111–122.

Banchs, R. E. (1997). Simulated annealing. Technical report, The University of Texas at Austin.

Bonyadi, M. R. and Michalewicz, Z. (2017). Particle swarm optimization for single objective continuous space problems: A review. *Evolutionary Computation*, 25(1):1–54.

Cai, J., Xu, G., Lu, H., Xu, C., Hu, Y., Cai, C., and Suo, J. (2022). Preparation of tritium breeding li2tio3 ceramic pebbles via newly developed piezoelectric micro-droplet jetting. *Journal of the American Ceramic Society*, 105.

Delahaye, D., Chaimatanan, S., and Mongeau, M. (2018). Simulated annealing: From basics to applications. pages 1–35.

Haralick, R. M. and Shapiro, L. G. (1992). *Computer and Robot Vision, Volume I*, pages 28–48. Addison-Wesley.

Hart, P. E. (2009). How the hough transform was invented [dsp history]. *IEEE Signal Processing Magazine*, 26(6):18–22.

Hernández, F. A., Arbeiter, F., Boccaccini, L. V., Bubelis, E., Chakin, V. P., Cristescu, I., Ghidersa, B. E., González, M., Hering, W., Hernández, T., Jin, X. Z., Kamlah, M., Kiss, B., Knitter, R., Kolb, M. H. H., Kurinskiy, P., Leys, O., Maione, I. A., Moscardini, M., Nádasi, G., Neuberger, H., Pereslavtsev, P., Pupeschi, S., Rolli, R., Ruck, S., Spagnuolo, G. A., Vladimirov, P. V., Zeile, C., and Zhou, G. (2018). Overview of the hcpb research activities in eurofusion. *IEEE Transactions on Plasma Science*, 46(6):2247–2261.

Heuser, J., Kolb, M., Bergfeldt, T., and Knitter, R. (2018). Long-term thermal stability of two-phased lithium orthosilicate/metatitanate ceramics. *Journal of Nuclear Materials*, 507:396–402.

Knitter, R., Alm, B., and Roth, G. (2007). Crystallisation and microstructure of lithium orthosilicate pebbles. *Journal of Nuclear Materials*, 367-370:1387–1392. Proceedings of the Twelfth International Conference on Fusion Reactor Materials (ICFRM-12).

Knitter, R., Chaudhuri, P., Feng, Y., Hoshino, T., and Yu, I.-K. (2013). Recent developments of solid breeder fabrication. *Journal of Nuclear Materials*, 442(1, Supplement 1):S420–S424. 15th International Conference on Fusion Reactor Materials.

Leys, O., Bergfeldt, T., Kolb, M. H., Knitter, R., and Goraieb, A. A. (2016). The reprocessing of advanced mixed lithium orthosilicate/metatitanate tritium breeder pebbles. *Fusion Engineering and Design*, 107:70–74.

Leys, O., Leys, J. M., and Knitter, R. (2021). Current status and future perspectives of eu ceramic breeder development. *Fusion Engineering and Design*, 164:112171.

Leys, O., Waibel, P., Matthes, J., and Knitter, R. (2019). Ceramic pebble production from the break-up of a molten laminar jet. In *Proc of ILASS Europe 2019: 29th Conference on Liquid Atomization and Spray Systems*.

Metropolis, N., Rosenbluth, A. W., Rosenbluth, M. N., Teller, A. H., and Teller, E. (1953). Equation of state calculations by fast computing machines. *The Journal of Chemical Physics*, 21(6):1087–1092.

Orfanidis, S. J. (1985). *Optimum signal processing : an introduction*. Macmillan, New York.

Otsu, N. (1979). A threshold selection method from gray-level histograms. *IEEE Transactions on Systems, Man, and Cybernetics*, 9(1):62–66.

Park, Y.-H., Cho, S., and Ahn, M.-Y. (2014). Fabrication of li2tio3 pebbles using pva–boric acid reaction for solid breeding materials. *Journal of Nuclear Materials*, 455(1):106–110. Proceedings of the 16th International Conference on Fusion Reactor Materials (ICFRM-16).

Pedersen, M. E. H. (2010). Good parameters for particle swarm optimization.

van Laarhoven, P. J. M. and Aarts, E. H. L. (1987). *Simulated annealing : theory and applications*. Kluwer Academic Publishers.

Vos, K. (2013). A fast implementation of burg's method. pages 2–4.

Zhang, M., Leys, O., Vogelbacher, M., Knitter, R., and Matthes, J. (2024). A high-speed camera-based measurement system for monitoring and controlling the induced jet break-up fabrication of advanced ceramic breeder pebbles. *The International Journal of Advanced Manufacturing Technology*.